ARTICLE

BIOTECHNOLOGY and BIOENGINEERING

Quantitative Characterization of Quantum Dot-Labeled Lambda Phage for *Escherichia coli* Detection

Peter B. Yim,[1] Matthew L. Clarke,[1] Michael McKinstry,[2] Silvia H. De Paoli Lacerda,[1] Leonard F. Pease III,[1,3] Marina A. Dobrovolskaia,[4] HyeongGon Kang,[1] Timothy D. Read,[5] Shanmuga Sozhamannan,[2] Jeeseong Hwang[1]

[1]National Institute of Standards and Technology, 100 Bureau Drive, Mailstop 8443, Gaithersburg, Maryland 20899; telephone: 301-975-4580; fax: 301-975-6991; e-mail: jch@nist.gov

[2]Biological Defense Research Directorate, Naval Medical Research Center, Silver Spring, Maryland

[3]Chemical Engineering Department, University of Utah, Salt Lake City, Utah

[4]Nanotechnology Characterization Laboratory, SAIC-Frederick/NCI-Frederick, Frederick, Maryland

[5]Department of Human Genetics, Division of Infectious Diseases, Emory University School of Medicine, Atlanta, Georgia

Received 28 May 2009; revision received 14 July 2009; accepted 17 July 2009

Published online 24 July 2009 in Wiley InterScience (www.interscience.wiley.com). DOI 10.1002/bit.22488

ABSTRACT: We characterize CdSe/ZnS quantum dot (QD) binding to genetically modified bacteriophage as a model for bacterial detection. Interactions among QDs, lambda (λ) phage, and *Escherichia coli* are examined by several cross-validated methods. Flow and image-based cytometry clarify fluorescent labeling of bacteria, with image-based cytometry additionally reporting the number of decorated phage bound to cells. Transmission electron microscopy, image-based cytometry, and electrospray differential mobility analysis allow quantization of QDs attached to each phage (4–17 QDs) and show that λ phage used in this study exhibits enhanced QD binding to the capsid by nearly a factor of four compared to bacteriophage T7. Additionally, the characterization methodology presented can be applied to the quantitative characterization of other fluorescent nanocrystal-biological conjugates.

Certain commercial equipment, instruments, or materials are identified in this paper to foster understanding and does not imply recommendation or endorsement by NIST, nor does it imply that the materials or equipment identified are necessarily the best available for the purpose. The views expressed in this article are those of the authors and do not necessarily reflect the official policy or position of the Department of the Navy, Department of Defense, nor the U.S. Government. The BDRD authors are employees of the U. S. Government. This work was prepared as part of their official duties. Title 17 U.S.C. §105 provides that "Copyright protection under this title is not available for any work of the United States Government." Title 17 U.S.C. §101 defines a U.S. Government work as a work prepared by a military service member or employee of the U.S. Government as part of that person's official duties.

Peter B. Yim and Matthew L. Clarke contributed equally to this work.

Correspondence to: J. Hwang

Contract grant sponsor: Defense Threat Reduction Agency

Contract grant sponsor: Department of Defense of the U.S. Government

Contract grant number: 8.10084_08

Biotechnol. Bioeng. 2009;104: 1059–1067.

Published 2009 Wiley Periodicals, Inc.

KEYWORDS: phage; bacteria detection; fluorescence; nanocrystal; microscopy; electron-spray differential mobility assay

Introduction

Bacterial detection plays a vital role in biological threat surveillance, agricultural safety, and medical diagnosis. While development of low cost, highly sensitive and selective bacterial detection platforms is of increasing interest, stringent validation of these typically qualitative techniques must be performed by quantitative analyses to precisely evaluate and improve methodologies and to standardize protocols. Faster detection speed is also necessary for real-world applications. To this end, rapid detections of bacteria in complex media have been demonstrated via fluorescently labeled antibodies or bacteriophage (Gibbs et al., 2004; Goodridge et al., 1999; Hahn et al., 2005; Mosier-Boss et al., 2003; Oda et al., 2004). Phage-based detection has the advantage of greater adaptability to fieldable assays due to broader environmental and storage stabilities of phages (Mosier-Boss et al., 2003). For detection methods, a

Published 2009 Wiley Periodicals, Inc. †*This article is a US Government work and, as such, is in the public domain in the United States of America.*

variety of optical techniques have been employed in an effort to quantify the assays. Fluorescence microscopy has been widely used with phages labeled with fluorescent antibodies or expressed with fluorescence protein chimeras, such as green fluorescence proteins fused to capsid proteins. A novel technique involving luminescent phage-associated lytic enzymes was demonstrated to detect and effectively kill pathogenic bacterial cells and to enable quantitative cell lysis assays (Schuch et al., 2002). However, assays involving organic fluorophores and chemiluminescent reagents often pose challenges to rigorous quantitative optical analysis at the single cell and single phage level due to environment-dependent or time-dependent signal-to-noise ratio changes such as background autofluorescence and photo-bleaching of the probes.

Here, we describe our efforts to quantitatively characterize the phage-based bacterial detection technique using fluorescent bio-nanoconjugates, specifically phage-quantum dot (QD) complexes. We select QDs for this assay as they have been used to detect and image biological molecules in vivo and in vitro due to their high photoluminescence, optical tunability and photostability compared to organic fluorophores (Alivisatos, 1996; Chan and Nie, 1998; Dubertret et al., 2002; Empedocles et al., 1996; Resch-Genger et al., 2008). Applying QD nanocrystal-phage complexes to target and detect *Escherichia coli* cells was demonstrated previously using T7 phage (Edgar et al., 2006). In brief, genetically modified parent T7 phage infected *E. coli* to yield progeny phages that were biotinylated by native *E. coli* BirA enzymes. Subsequently, streptavidin-coated QDs were conjugated to the progeny phage, which bind to other target *E. coli*. Fluorescence imaging of single cells, single phage, and single QDs was demonstrated. However, the use of lytic T7 phage complicates the rigorous quantitative analysis of the cell–phage interaction due to continuous lysis of cells at the end of the phage replication life cycle resulting in reduced target cell counts and increased amounts of cell fragments. Furthermore, even under conditions of excess QDs during the detection assay, on average only about two QDs were conjugated to the phage capsid. This low conjugation efficiency between QDs and T7 phage may be attributed to the fact that the accessible level of endogenous BirA enzymes is diffusion-limited and/or may not be sufficient to biotinylate the highly expressed capsid protein in the short time before cell lysis in the lytic cycle of the T7 phage. Additionally, cell lysis induced by lysogenic T7 bacteriophage may hinder the interaction between QDs and phage targeted onto a bacterial cell in the subsequent detection assay.

As quantitative characterization of the QD-phage-bacteria complex is essential to the understanding and validation of bacteriophage-based detection assays, this study focuses on quantitative characterization using temperature sensitive mutant bacteriophage lambda (or λ phage) gt11 as a model. Bacteriophage λ is a temperate phage with a double-stranded (ds) genome of ~48 kb encapsulated in an icosahedral capsid (~50 nm in diameter) with a long and fibrous tail (~150 nm in length). The λ capsid is composed of two major coat proteins, gpE and gpD. Lambda capsid maturation begins with the formation of the prohead, composed solely of gpE. As the genomic DNA is packaged, the capsid expands in volume by ~45% and ~405 copies of gpD are then added to fully populate and stabilize the capsid. GpD is a 109 amino acid protein (excluding the initial methionine which is removed from the mature protein) and is required for the packaging of full-length genomes. Bacteriophage λ has been shown to be able to accommodate the display of foreign peptides and proteins on the gpD major coat protein (Zanghi et al., 2005 and references therein). Bacteriophage λ was chosen because it is one of the most studied organisms and its binding to *E. coli*, via receptor LamB, has been well characterized (Murray and Gann, 2007). To employ λ phage for this assay, the following modifications to the previous protocol involving the T7 phage assay were implemented. In brief, (1) to biotinylate λ phage, we genetically engineered the λ genome to express a biotin binding peptide on the capsid surface as a *gpD* fusion in a temperature sensitive lysogen; (2) upon adsorbing the phage to cells at room temperature, the induction of the lysogen by a temperature elevation resulted in phage that are biotinylated due to the addition of biotin moieties to the biotin binding peptide on the capsid proteins by endogenous *E. coli* BirA enzymes; (3) after harvesting these biotinylated phage, for the final cell targeting, the room temperature binding assay allows adsorption of biotinylated λ phage yet prevents replication inside the cell and subsequent lysis during the assay. A diagram illustrating the detection method is presented in Figure 1.

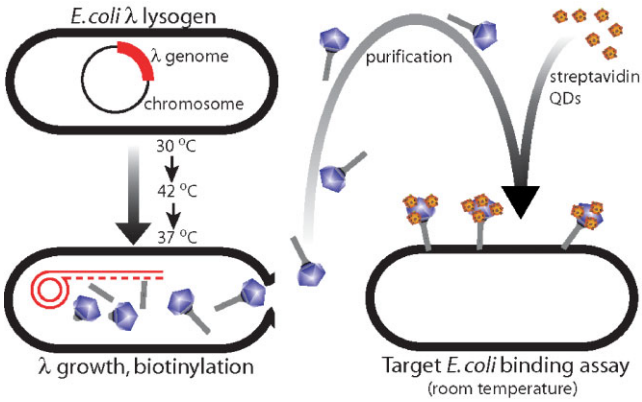

Figure 1. Bacterial detection strategy using biotinylated λ phage-streptavidin QD complexes. The genome of a temperature sensitive λ phage in a lysogen (shown in red on black chromosome) was modified to express a biotin binding peptide on the capsid surface. Induction of the lysogen by a temperature shift during bacterial growth resulted in a λ phage lysate that has biotin added to the biotin binding peptide on the capsid surface by the bacterial BirA enzyme. The lysed bacteriophage λ were collected and used for bacterial binding assay. Streptavidin quantum dots were conjugated to biotinylate bacteriophage λ which in turn targets the bacteria at room temperature. The QD-bacteriophage-bacteria complex can then be analyzed by multiple methods.

For quantitative assessment, important factors to consider include the number of QDs bound to each phage and the number of phages bound to each bacterium. The above strategy involving mutant λ phage provides an advantage for quantitative analysis of cell–phage interactions as well as phage–QD interactions due to the ability to maintain the lysogenic state of the infected cells indefinitely during analysis at room temperature. This permits precise counting of the cells or measurement of QD fluorescence intermittency without concern for cell lysis events. Control experiments were conducted using wild-type λ phages which lack the biotin binding peptide gene and allow cell binding without replication and lysis of the bacterium. In the remainder of this letter, we demonstrate the cross validation of several quantitative measurements to characterize QD-conjugated bacteriophage λ binding to *E. coli* at the single cell, single phage, and single QD level. First, flow and image-based cytometry provide measurements of the labeled bacteria fluorescence intensities. We deduce the number of phage bound to each bacterium by image-based cytometry. We then determine the number of QDs attached to each phage using quantitative fluorescence microscopy, transmission electron microscopy (TEM), and electrospray differential mobility analysis (ES-DMA).

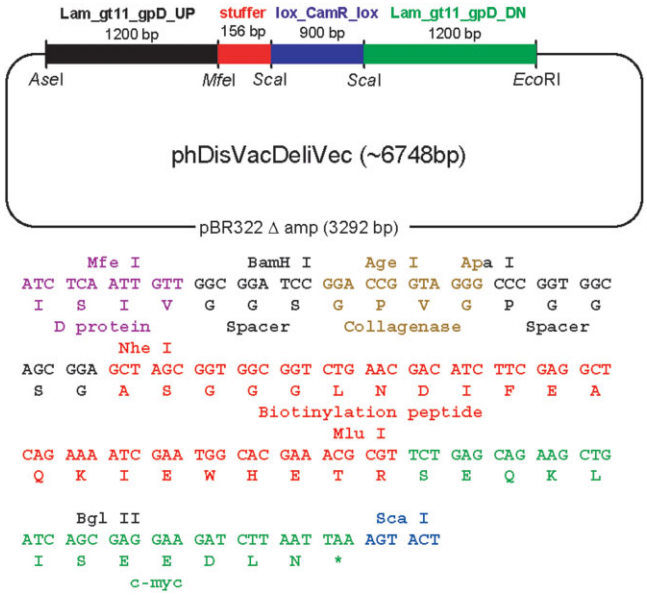

Figure 2. Top panel shows the structure of the plasmid used for construction of the *gpD::bio* fusion. The bottom panel shows the DNA sequence of the 156 stuffer fragment carrying the 3′ end of *gpD* and the bio peptide fusion junction (Gupta et al., 2003). [Color figure can be seen in the online version of this article, available at www.interscience.wiley.com.]

Materials and Methods

Construction of λ gt11 *gpD::bio* Phage

λ gt11 *gpD::bio* (recombinant phage with *gpD*-biotin binding peptide fusion) was constructed by linear DNA transformation of a polymerase chain reaction (PCR) fragment carrying the *gpD::bio* fusion and a Cam^r marker flanked by the *gpD* upstream and downstream sequences. This fragment was derived from a plasmid designated as phDisVacDeliVec (Fig. 2). In order to construct this vector, a 1,196 bp fragment of λ carrying the Nu3 gene, λ sequences upstream of *gpD* gene, from positions 4880 to 6097 was synthesized and cloned into a vector resulting in pGOv3-NV3 (Gene Oracle, Inc. Mountain View, CA). An *Ase*I–*Mfe*I fragment carrying this fragment was cloned into a fragment of pBR322, which was PCR amplified with 5′-GGGCCCCAATTGAGTACTGAATTCTCATGTTTGACAGCTTATCATCG-3′ (pBR322 sequences underlined 4–26) and 5′-GGGCCCATTAATCTGTCAGACCAAGTTTACTCATATA-3′ (pBR322 sequences underlined 3268–3292) with those two sites at the extremities resulting in pMM101. A synthetic 146 base pair *Mfe*I–*Sca*I fragment from pDrive NV2 (Gene Oracle, Inc.) containing sequences for the biotinylation peptide (see Fig. 2 for the sequence and Gupta et al., 2003) was ligated to the *Mfe*I–*Ase*I sites of pMM101, resulting in pMM102. This fragment designated as the stuffer in Figure 2 encodes the end of gpD protein without the stop codon (amino acids ISIV) followed by a spacer and then collagenase peptide cleavage motif (GPVG) in order to cleave off the displayed protein or peptide if so desired, followed by another spacer and biotinylation peptide and c-myc peptide. The c-myc is a deca peptide and allows quantification of the displayed proteins by Western blot using monoclonal antibody, 9E10.

The 1,110 bp *Sca*I–*Eco*RI fragment from bacteriophage λ (nt 6,080–7,186), containing sequences downstream of *gpD* and *gpE*, was PCR amplified using primers 5′-AATATTAGTACTCTTTACCCTTCATCACTAAAGGCC-3′ and 5′-GGGCCCGAATTCGAAACAATGGCCCCGAAGGGCCAT G-3′ and ligated to *Sca*I–*Eco*RI digested pMM102 resulting in pMM103. A 900 bp chloromphenicol acetyl transferase gene encoding (Cam^r) was PCR amplified from a pOmega L derivative (Pomerantsev et al., 2006), blunted and ligated to *Sca*I site in pMM103 resulting in pMM104. A fragment carrying the *gpD* up-stuffer-Cam^r and *gpD_dn* sequences was PCR amplified from pMM104 using primers 5′-GGGCCCATTAATGAGAAGAGTGACA GCAGAGCTGCG-3′ and 5′-GGGCCCGAATTCGAAACAATGGCCCCGAAGGGCCATG-3′ and transformed into KM22/λ gt11::*tet* selecting for chloramphenicol resistance. KM22 is a derivative of *AB1157thr-1 leu-6 thi-1 lacY1 galK2 ara-14 xyl-5 mtl-1 proA2 his-4 argE3 str-31 tsx-33 supE44 rec*+D(*recC ptr recB recD*)::P*lac-bet exo kan* (Murphy, 1998) and λ gt11::*tet* carries a *tet* gene in the *Eco*RI site in λ gt11 (this study). The CamR colonies were verified by PCR and sequencing the *gpD* region. The resulting λ lysogen, upon induction at 42°C produced λ phage particles with capsids displaying biotinylated gpD fusion protein. Biotin binding peptide expression on the recombinant phage capsid protein was confirmed by Western blot (data not

shown). In the Western blot, the parent λ gt11 lysate exhibited only a band at 17 kDa corresponding to biotin carboxyl carrier protein (BCCP) enodgenous to *E. coli*. Recombinant bacteriophage λ *gpD::bio* lysates exhibited a 15.6 kDa protein corresponding to biotinylated gpD fusion protein in addition to the endogenous BCCP, indicating that biotinylated gpD has been incorporated in the phage capsid.

Bacteriophage λ Binding

Biotinylated bacteriophage λ was added to an *E. coli* K12 ER1793 [F-*fhuA2 Δ(lacZ)r1 glnV44 e14-(McrA-) trp-31 his-1 rpsL104 xyl-7 mtl-2 metB1 Δ(mcrC-mrr)114::IS10* (Waite-Rees et al., 1991)] solution at various phage-cell ratios. To obtain optimal results for both flow and image-based cytometry, we carefully balanced the phage-cell ratio. We set this pre-binding ratio to 100 so the post-binding ratio (herein defined as the multiplicity of infection or MOI) allows for counting of phages on individual *E. coli* cells using far-field optical microscopy. Higher densities of phages per cell would occlude quantitative measurement due to spatially irresolvable distributions of fluorescent signals from phage-QD complexes on a cell due to the intrinsic diffraction limit of far-field optical microscopy. In a typical experiment, 6.5 μL of phage (1.0×10^{11} phage/mL) was added to 10.0 μL of *E. coli* (6.5×10^{8} cells/mL) and incubated by gentle rocking at room temperature (21°C) for 15 min. Streptavidin-labeled QDs (1.1 μL at 1 μmol/L, 605 nm emission, Invitrogen, Carlsbad, CA) were added at a concentration QD/phage ratio of 1,000:1. After 15 min of room temperature incubation, the sample was filtered via 0.45 μm pore size microcentrifuge spin columns to remove free QDs and unbound bacteriophage λ. Membrane-retained cells were resuspended in phosphate buffered saline (PBS) buffer for further analyses.

Flow Cytometry

Bacterial cell-phage-QD complexes were treated with 0.5% glutaraldehyde prior to measurement to reinforce the cell membrane, and diluted 1:10 in PBS and passed through cell strainer caps into polystyrene tubes (BD Falcon 352235) immediately prior to analysis on the flow cytometer. The 488 nm laser line of the flow cytometer (BD Biosciences, FACSCalibur, Franklin Lakes, NJ) was used to excite QDs conjugated to λ phage. QD fluorescence was detected on the second fluorescence channel (FL2), with the manufacturer's 585 ± 42 nm band pass filter setting. Detailed instrument settings and gating have been reported previously (Yim et al., 2007). Data acquisition and analysis were performed using Cell Quest Pro software (BD Biosciences).

Image-Based Cytometry

QD-phage-*E. coli* complexes in PBS were dispersed and attached to #1.5 coverslips cleaned using potassium hydroxide and ozone. Samples were imaged using an IX81 epi-fluorescence microscope (Olympus America, Inc., Center Valley, PA) with a differential interference contrast (DIC) attachment and an electron multiplying charged coupled device (EM-CCD) camera (Andor Technology, Belfast, UK). Simultaneous multimodal imaging of the DIC and fluorescence images was performed using a Dual-View multichannel imager (Photometrics, Tuscon, AZ). To eliminate spectral overlap, DIC imaging was performed using white light illumination passed through a 680 nm long pass filter, while QDs were excited with the 457 nm from an argon laser (Coherent, Santa Clara, CA) guided through an optical fiber to an oil immersion objective lens (1.45 NA 60×, Olympus America, Inc.) in a pseudo total internal reflection fluorescence (pseudo-TIRF) microscopy configuration where fluorescence excitation is confined to ~1 μm depth from the substrate (Cui et al., 2007). To assess the time-dependent optical characteristics of QDs, we collected images with 25 ms exposure times for 500 frames.

To determine the MOI for each bacterium, cell boundaries were identified by applying a Sobel edge-finding algorithm to the DIC image. Edges were dilated to ensure counting of fluorescent spots near the cell boundary. We applied a Gaussian point-spread function (obtained from individual QD signals on the substrate surface) and a sequence of bandpass and neighborhood filters to the fluorescence image. The local fluorescence maxima existing within the perimeter of the bacteria cells determined by DIC are returned.

Transmission Electron Microscopy

The phage-QD complexes were prepared adding 1.2 μL of streptavidin QDs (1 μmol/L) to 20 μL of phage (*gpD::bio*, 3.5×10^{10} phage/mL) and incubating by rocking at room temperature (21°C) for 20 min. Water (400 μL) was added to the vial, and filtered by centrifuge at 2,000 rpm for 50 min using 100,000 MWCO membrane centrifuge filters (Sigma, St. Louis, MO). This step was repeated twice more using new filters each time. Finally, TEM samples were prepared by dropping diluted solutions onto carbon-coated copper grids. The complexes were measured by transmission electron microscope (Philips 400T) operating at 120 KV equipped with a Soft Imaging System CCD camera (Cantega 2K).

Electrospray Differential Mobility Analysis

To achieve optimal conductivity for electrospray, the streptavidin-coated QDs (1.0×10^{13} particles/mL), biotinylated λ phages (1.0×10^{10} phage/mL), and QD-phage complexes (1.0×10^{10} phage/mL in PBS prior to biotinylation and mixing) were dialyzed to minimize nonvolatile salts and increase the concentration of the phage samples. The QD sample was dialyzed for one week into a 2.0 mmol/L ammonium acetate solution at pH 8 with a slide-a-lyzer

cartridge (Pierce Biotechnology, Rockford, IL) having a 10 kDa molecular weight cut off. The two phage samples were dialyzed against Nanopure water (Millipore, Billerica, MA) using Spectra/Por Float-A-Lyzer tubing, MWCO 100,000 (Spectrum Laboratories, Rancho Dominguez, CA) for 3 days. The phage samples were further concentrated 10-fold using spin columns for 16–18 min at 3,000 rpm, bringing their concentration above the ES-DMA's minimum detection limit. These solutions were transferred to low protein binding 1.5 mL microcentrifuge tubes (Eppendorf, Westbury, NY) and the phage samples were stored under refrigeration at 4°C. The ES-DMA experimental method is described in detail elsewhere (Pease et al., 2007).

Modeling linking the experimental mobility to the particle size has been detailed previously (Mulholland et al., 2006; Pease et al., 2007, 2008). The spherically equivalent size, termed the mobility diameter (d_m), for several structures were calculated in Mathematica (version 6.0, Wolfram Research, Inc., Champaign, IL) using the projected area formalism introduced by Pease et al. (2007), who show that the mobility diameter may be determined from the projected areas, A_i, with

$$d_m = \left(\frac{\sqrt{\pi}}{6} \sum_{i=1}^{3} A_i^{-1/2} \right)^{-1}. \quad (1)$$

Calculations to predict the mobility diameter of the QD-labeled phage assume the icosahedral head to be a sphere and the QDs to be right cylinders 18.2 nm in length and 11.5 nm in diameter. The rigid rods are assumed to be tangent to the sphere and the rod's axis of symmetry lies parallel with the sphere's nearest tangent plane. To employ Equation (1), only sphere-rod systems with sufficient symmetry to facilitate straightforward identification of the particle system's principle axes were considered. For more complicated geometries where faces of the rods do not align with the particle's coordinate system, a gravimetric approach was used to determine the projected areas: a structure and its three orthogonal projections were assembled in Mathematica, the projection was printed and cropped, and the relevant areas were determined assuming the paper to be of uniform density and thickness. This latter approach introduces minimal uncertainty when compared to direct geometric calculation.

Results and Discussion

We first analyze the binding of QD-decorated phages to the bacteria by flow cytometry. This rapid, high throughput technique is capable of quantifying populations of targeted versus untargeted cells and has previously been applied to the detection of fluorescently tagged bacteria (Hahn et al., 2008; Yamaguchi et al., 2003). We use flow cytometry to ensure that biotinylated λ phage are responsible for fluorescent labeling of the bacteria (i.e., QDs do not bind nonspecifically but rather attach to cells via the bacteriophage "linker"). To this end, bacterial cells incubated without QDs or phages were analyzed to establish the background counts and fluorescence threshold. Here, as discussed elsewhere, the threshold of fluorescence intensity is $m + 3\sigma$, where m is the mean background fluorescence intensity and σ is the standard deviation of the Poisson distribution of the background noise (Krogmeier and Hwang, 2005; Krogmeier et al., 2008). Cells incubated with QDs but without phages were then examined (Fig. 3a); no significant shift in fluorescence signals from the cells in the scatter plot was observed, confirming nonspecific binding of QDs with *E. coli* to be negligible. Next, *E. coli* cells mixed with QDs and non-biotinylated wild-type λ phage were analyzed (Fig. 3b), and we observed similar signals compared to the sample without phage. When cells incubated with QDs in the presence of biotinylated bacteriophage were analyzed,

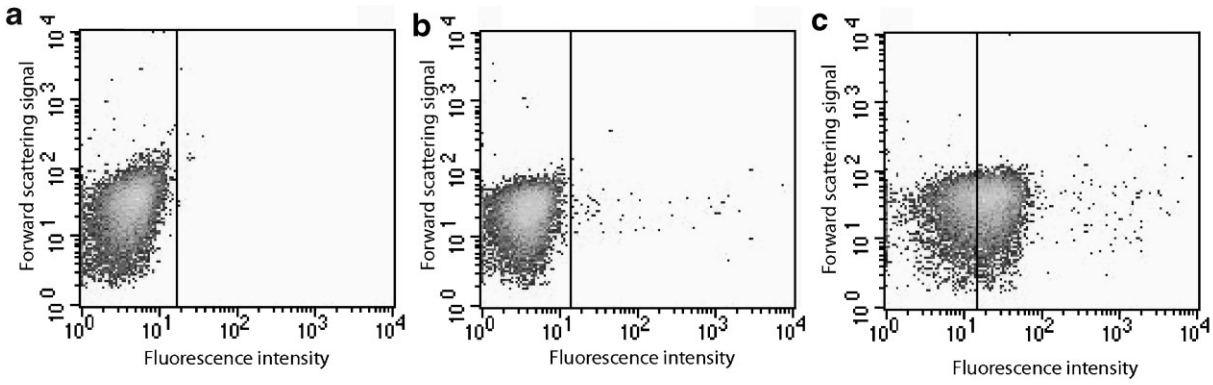

Figure 3. Detection of QD-phage binding to *E. coli* using flow cytometry. Forward light scattering versus fluorescence intensity graphs of (**a**) *E. coli* and streptavidin QDs (1,000× the number of *E. coli*), (**b**) *E. coli*, wild-type non-biotinylated bacteriophage λ (100× the number of *E. coli*), streptavidin QDs (1,000× the number of bacteriophage λ), and (**c**) *E. coli*, biotinylated bacteriophage λ (100× the number of *E. coli*), streptavidin QDs (1,000× the number of biotinylated bacteriophage λ). Solid lines on the scatter plots indicate the threshold determined in (a). The populations above the threshold for the three graphs are 0.08%, 0.56%, and 58.77%, respectively.

the population of cells with fluorescence intensities above the threshold greatly increases (Fig. 3c) while the forward light scattering signals remained similar to the two previous control results, suggesting that conjugation does not induce cell aggregation. Comparing the non-biotinylated and biotinylated phage in Figure 3b and c, we confirm that biotinylation is required to produce QD tagged *E. coli*. However, ≈42% of the population in this latter case retains fluorescence signals below the threshold, indicating that these cells may not have been labeled with QDs or that the labeling of some cells was below the sensitivity of the instrument. While higher labeling efficiencies would be required for sensitive detection of bacteria by flow cytometry, the degree of labeling here demands more detailed analysis of the QD-decoration of the phage by other methods described below.

Characterization of the QD-phage conjugation and a detailed understanding of the phage-QD labeling of *E. coli* was obtained through an image-based cytometry technique based on simultaneous fluorescence and bright-field optical microscopy. Although conventional flow cytometry is able to measure the optical properties of single cells at a rate of 1,000 or more cells per minute, it has a limited capability for mapping individual events with quantitative details. In fact, to accurately quantify cellular and sub-cellular characteristics, image-based cytometry has recently and rapidly emerged (Carpenter et al., 2006). In this technique, images of single cells obtained with fluorescence microscopy provide exact information on signal intensity, location and distribution of specific molecules within cells in vitro or in vivo (e.g., in tissues or monolayers), allowing for the dynamic investigation of cellular properties in response to the cell's microenvironment. Here, the position of *E. coli* cells is visualized by differential interference contrast (DIC, Fig. 4a), and QD-phage labeling is determined using pseudo-TIRF microscopy (Fig. 4b). To approach the high-throughput aspect of conventional flow cytometry, automated image analysis was performed in MATLAB to quantitatively analyze the fluorescence signals attributed to phage-QD complexes bound to *E. coli*.

Our first interest is in automatic determination of the MOI, the average number of λ phage bound to each targeted *E. coli* cell. The number of local fluorescence maxima within the perimeter of the bacterial cells represent the number of phage-QD complexes as indicated in Figure 4c. Based on the modest phage concentration and the low density of fluorescence spots observed on the cells, it was assumed for the purposes of this estimation that only one labeled phage was present within each fluorescent spot. We find that approximately half of the cells have been labeled by QD-phage complexes when incubated at a phage-to-cell ratio of 100; experiments incubated at lower phage-to-cell ratios result in fewer numbers of labeled cells (Fig. 4d). When the same image analysis was performed on cells incubated with

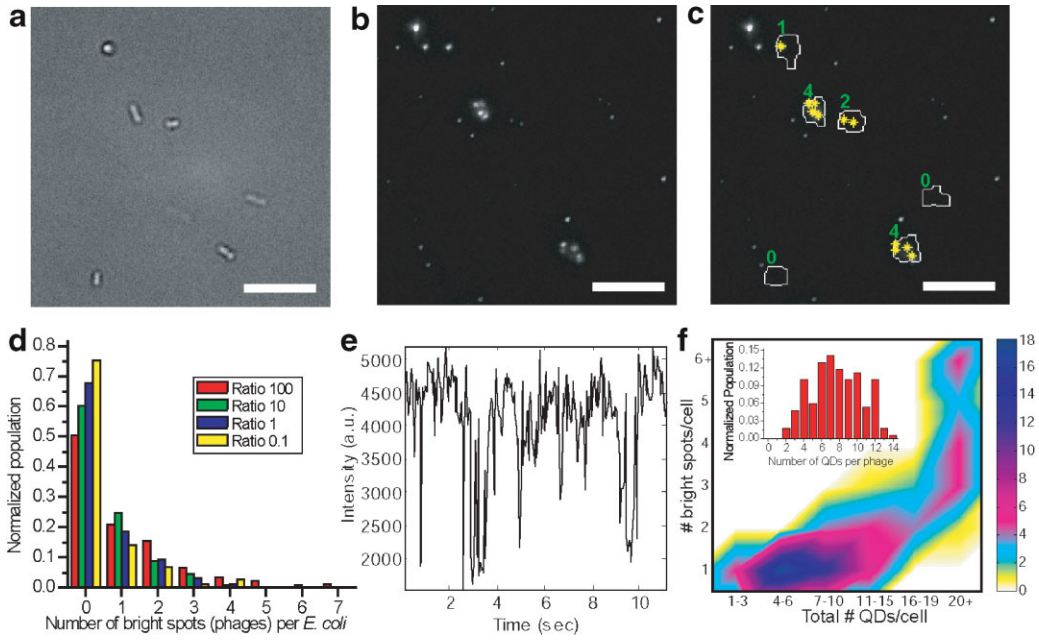

Figure 4. Imaged-based cytometry example images and data (scale bars are 10 μm). **a**: DIC image of several *E. coli*. **b**: Fluorescence image of the same area using 457 nm excitation with 25 ms exposure. **c**: Final counting result with enlarged outlines of cell found by processing image (a) and deconvoluting local maxima of image (b) within those outlines. Numbers designate the number of bright spots per outline with local maxima indicated by yellow asterisks. **d**: Histogram of the normalized frequency versus the number of bright spots per *E. coli* for several phage/cell ratios (~100 cells analyzed per ratio). **e**: Representative fluorescence intensity fluctuation caused by stochastic blinking of an individual QD. **f**: 3D histogram comparing the number of bright spots per cell and the total number of QDs per cell. Counts from unlabeled cells (119 cells) are not shown for clarity. Inset: Normalized histogram of the number of QDs per phage deduced from image processing and analysis.

streptavidin-QDs but without phage, no cells with fluorescence labeling were observed (data not shown), confirming that nonspecific binding and residual free QDs have little to no impact on these results.

Further analysis was performed on each fluorescent spot within the bacterial cell boundary to estimate the number of QDs present per phage. An example of the time trace of the fluorescence intensity at a local maximum from a single QD is presented Figure 4e. The quantized blinking from the QD ($m = 1$, see equation below) present within this spot was observed. While it is possible to determine the number of QDs based on this fluorescence intermittency, it is very challenging for more than three interacting QDs as their stochastic blinking behaviors obscure the quantized levels. Many observed bright spots of QD-tagged phage had average fluorescence intensities higher than three times the average single QD intensity, and the quantized blinking behavior was obscured due to the non-synchronized blinking behavior of individual QDs. For this reason the intensity of the fluorescence was examined to estimate the number of QDs per spot. To a first-order approximation, the number of "blinking" QDs within each bright spot (phage) can be estimated from the ratio of the total time-averaged integral of the fluorescence intermittency, $I^{\text{all-on}}(t)$, from multiple QDs all in on states, to the time-averaged integral of the fluorescence intermittency from a known number of QDs (determined from the number of quantized blinking levels, m), $I'^{\text{all-on}}(t)$, located near the substrate surface ($z \leq 50$ nm) as

$$\#\text{QDs per bright spot(phage)} = \varepsilon \frac{(1/N)\sum_i (1/(T_i - T_{i-1})) \int_{T_{i-1}}^{T_i} [I_i^{\text{all-on}}(t) - \langle I_i^{\text{off}}(t)\rangle]\mathrm{d}t}{(1/m)(1/N)\sum_i (1/(T_i - T_{i-1})) \int_{T_{i-1}}^{T_i} [I_i'^{\text{all-on}}(t) - \langle I_i'^{\text{off}}(t)\rangle]dt}. \quad (2)$$

In this equation, T_i represents the time interval during the ith time period when all the QDs are in an on state, and N is the total number of time intervals when all the QDs are in on states. The correction factor, ε, incorporates a variety of phenomena including changes in photoluminescence as a result of different chemical environments, fluorescence quenching due to photo-bleaching, and variation in the excitation field intensity which depends on the z location of phage-QD complexes in the pseudo-TIRF excitation field. The counting algorithm was performed on 14 images (~200 cells) and a 3D histogram of the population of cells as a function of the number of bright spots per cell versus the estimated total number of QDs per cell (over all bright spots/phages) is shown in Figure 4f. Cells targeted with more than one labeled phage exhibit a substantial number of QDs. Examining the spots individually finds an average of 7 ± 3 QDs per phage ($n = 170$, see inset of Fig. 4f). This value is at least three times as many QDs bound to the biotinylated phage in the T7 assay (Edgar et al., 2006). Additionally, we should note that while such time-based measurements would be very challenging in systems undergoing phage-induced cell lysis they were readily performed using the mutant λ phage; no lysis was observed by bright field microscopy during the analysis.

Systemic uncertainty in the above estimate of QDs/cell derives primarily from the setup of the image-based cytometer and the constraints used within the image processing. Under pseudo-TIRF illumination, where the field intensity decays away from the substrate surface, the emission intensity of a phage-QD complex on a cell surface depends on its distance above the substrate surface. Accordingly, some of the bright spots away from the substrate surface (e.g., on the upper portion of the cell) are not effectively excited due to the decaying field and may not emit enough photons to be found by our image processing procedure, which selects phage-QD complexes only with local maximum values $>3\sigma$ from the background noise. For instance, the total population of the cells found by image-based cytometry that do not exhibit fluorescence labeling is ~60%. Although the fluorescence microscopy sensitivity is higher than that of conventional flow cytometry (Yim et al., 2007), the number of unlabeled cells evaluated here by image-based cytometry is higher than the flow cytometry result, suggesting that our image processing methods have sacrificed total fluorescence intensity in favor of detailed analysis of those phage-QD complexes within the excitation field.

Since determination of the number of QDs by fluorescence measurements can be influenced by experimental conditions, we further measured the number of QDs per phage by TEM and ES-DMA. One distinct advantage of QDs over conventional organics dyes is their high electron density. This allows for dual use as a fluorescence and electron microscopy labeling agent (Giepmans, 2008). Whereas it is extremely challenging to determine the number of organic fluorescent molecules on a target complex from imaging, TEM can be used directly to determine the number of QDs per phage independent of the QD's photoluminescence. Indeed, QD decoration of the phage capsid could be readily verified by TEM (Fig. 5A). Additionally, to further confirm that the QD-decoration of the phage did not disrupt phage-*E. coli* binding, TEM on the QD-phage-bacteria complex was performed. For example, a single λ phage with several QDs conjugated to its capsid. Attaching to the *E coli* by a curved tail is observed in

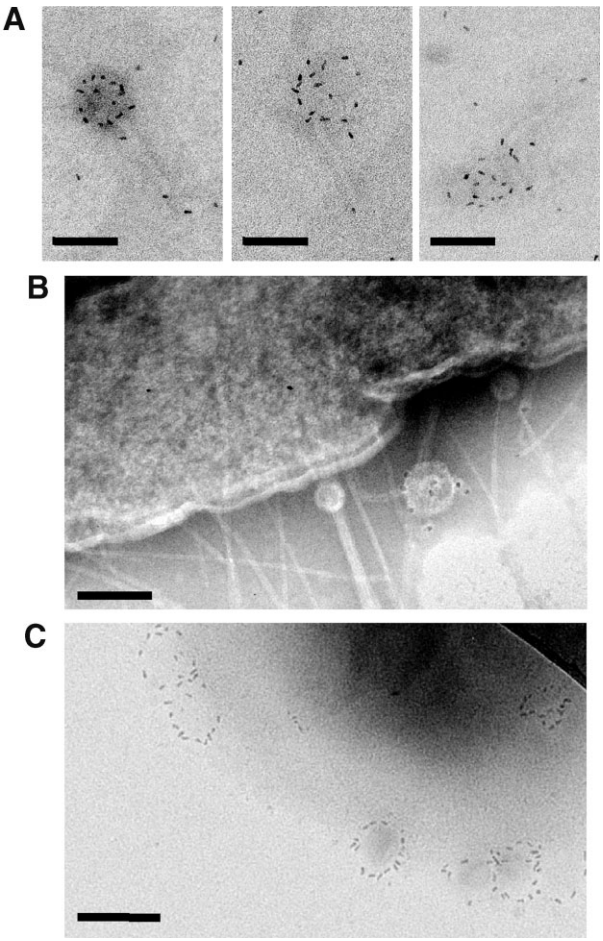

Figure 5. **A**: TEM images of biotinylated bacteriophage λ (gt11 *gpD::bio*)-QD complexes on custom prepared carbon surfaces without staining. Streptavidin-coated QDs (dark spots) were identified through the oblong shapes of the CdSe/ZnS core. Free QDs on the carbon surface are observable in the image. **B** and **C**: TEM images of a biotinylated bacteriophage λ (gt11 *gpD::bio*)-QD complex binding to *E. coli*. Phage binding in (C) is deduced by the circular decoration of QDs. Scale bars are 100 nm.

Figure 5B. Multiple phage binding to single *E. coli* was readily confirmed (Fig. 5C), especially when higher phage ratios were used. Manually counting QDs around each phage in TEM images we determined that 13 ± 4 ($n = 175$) QDs were bound to each phage. Wild-type phage did bind bacteria, yet QDs were absent from these images.

Due to concern over possible skewing of the TEM counts as a result of potential substrate drying effects (Fischer, 2002) and potential bias of the size distributions due to the difficulty of directly observing phages with fewer QDs, we also characterize the phage-QD conjugates by ES-DMA. This technique can determine the size of nanoparticles to subnanometer resolution with a large sample throughput (in excess of tens of thousands of particles per hour). We first aerosolize and charge the particles (e.g., viruses, QDs, and virus-QD complexes) using electrospray. We then set the charge on the particles in the gas phase by passing them through a bipolar charger to give them a distribution dominated by +1, neutral and −1 charge states (Wiedensohler, 1988). Similar to mass spectrometry, DMA then separates aerosolized particles based on their charge-to-size ratio. Because DMA only analyzes positively charged particles, the charge is fixed to essentially +1, and our system in turn directly separates the particles based on their size. Individual size-separated particles were counted using a condensation particle counter (CPC).

After characterizing the size of the individual QD and the λ phage capsid (data not shown; separate paper in preparation), the number of QDs added to the bacteriophage λ could be deduced from ES-DMA size distributions. Figure 6 compares a histogram for the QD-phage complex to the phage alone. The phage peak centers at 48.8 nm while the QD-phage complex is shifted by 7.0 nm to 55.8 nm due to the addition of the QDs. We can estimate the typical number of QDs attached to a λ phage head by assuming the icosahedral head of the virus to be a sphere and the QDs to be a cylinder with dimensions that account for the streptavidin coating. In depth details of ES-DMA theory and analysis of these conjugates will be published separately, but calculations using average sizes of QDs and phage estimate a mobility diameter of 55.8 nm corresponds to 5 to 6 attached QDs per phage. This average result strongly agrees with the fluorescence measurements, and, as expected, is lower than that deduced by TEM. We note with interest that calculations comparing the lower limit of the phage distribution to the upper limit of the QD-phage distribution leads to an estimate of 13–14 QDs. The TEM measurements lie within this range and therefore we can conclude that the contribution of limited artifacts in the TEM analysis falls in the values found in ES-DMA size distributions.

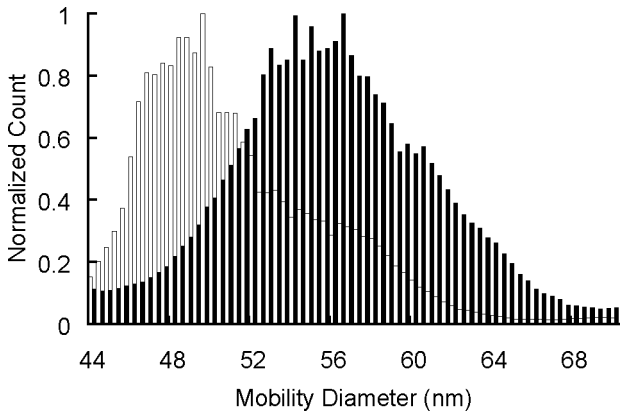

Figure 6. Histograms from ES-DMA showing the frequency of collection of particles at specific mobility diameters (i.e., assuming a spherically equivalent aerodynamic size) for λ phage (empty bars) and biotinylated λ-phage labeled with streptavidin-coated QDs (filled bars). The samples are electrosprayed into a gas flow of 1.0 L/min of air and 0.2 L/min of CO_2 via a 25 μm inner diameter capillary. The bipolar neutralizer houses a Po-210 source. The sheath flow rate in the DMA is set to 30 L/min. The flow rate in the CPC is set to 1.5 L/min and counts are averaged over 20 s or 500 cm^3 of gas flow. The histogram is binned at 0.4 nm.

Conclusion

Comparison between the techniques shows that, while the number of QDs bound to λ phage has been improved on average compared to that for T7 phage, there is a significant variation in the number of QDs bound to each phage. However, cells targeted with more than one QD-phage complex can be readily observed by flow cytometry or fluorescence microscopy due to increased number of QDs per phage. We have demonstrated the application of the temperature-sensitive mutant λ phage, and the precise assessment by thorough analysis and time-based measurements without concern for phage induced cell lysis skewing the data. Furthermore, these results revealed the detailed information available when combining multiple techniques to characterize nanoparticle decoration of biological structures. Our integrated approach of fluorescence microscopy and image-based cytometry provides a bridge between the high-throughput cellular level analysis provided by flow cytometry and the nanometer scale of electron microscopy. Additionally, results from ES-DMA, which has the capabilities of both high-throughput evaluation and nanoscale characterization, corroborate the degree of QD-binding to the phage capsid observed by both fluorescence and electron microscopies.

The authors thank Dr. Georgeta Crivat, Dr. Zhenping Zhou, Dr. Jianyong Tang, Dr. John Woodward, Dr. Lori Goldner, Dr. Garnett Bryant, and Dr. Paul DeRose at NIST; and Dr. Anil Patri at the Nanotechnology Characterization Laboratory (NCL) at SAIC-Frederick/NCI-Frederick and Daniel Nelson at the University of Maryland Biotechnology Institute for useful discussions and acknowledge Mike Zachariah, Mike Tarlov, and De-Hao Tsai for their assistance with ES-DMA training. JH was supported by the National Institute of Standards and Technology Advanced Technology Program. MC was supported by the NRC postdoctoral fellowship program. This work was supported by funds from the Defense Threat Reduction Agency, Department of Defense of the U.S. Government (BDRD authors; grant # 8.10084_08_NM_B).

References

Alivisatos AP. 1996. Semiconductor clusters, nanocrystals, and quantum dots. Science 271(5251):933–937.

Carpenter AE, Jones TR, Lamprecht MR, Clarke C, Kang IH, Friman O, Guertin DA, Chang JH, Lindquist RA, Moffat J, Golland P, Sabatini DM. 2006. Cellprofiler: Image analysis software for identifying and quantifying cell phenotypes. Genome Biol 7(10):R100.

Chan WCW, Nie SM. 1998. Quantum dot bioconjugates for ultrasensitive nonisotopic detection. Science 281(5385):2016–2018.

Cui BX, Wu CB, Chen L, Ramirez A, Bearer EL, Li WP, Mobley WC, Chu S. 2007. One at a time, live tracking of NGF axonal transport using quantum dots. Proc Natl Acad Sci USA 104(34):13666–13671.

Dubertret B, Skourides P, Norris DJ, Noireaux V, Brivanlou AH, Libchaber A. 2002. In vivo imaging of quantum dots encapsulated in phospholipid micelles. Science 298(5599):1759–1762.

Edgar R, McKinstry M, Hwang J, Oppenheim AB, Fekete RA, Giulian G, Merril C, Nagashima K, Adhya S. 2006. High-sensitivity bacterial detection using biotin-tagged phage and quantum-dot nanocomplexes. Proc Natl Acad Sci USA 103(13):4841–4845.

Empedocles SA, Norris DJ, Bawendi MG. 1996. Photoluminescence spectroscopy of single CdSe nanocrystallite quantum dots. Phys Rev Lett 77(18):3873–3876.

Fischer BJ. 2002. Particle convection in an evaporating colloidal droplet. Langmuir 18(1):60–67.

Gibbs KA, Isaac DD, Xu J, Hendrix RW, Silhavy TJ, Theriot JA. 2004. Complex spatial distribution and dynamics of an abundant *Escherichia coli* outer membrane protein, LamB. Mol Microbiol 53(6):1771–1783.

Giepmans BNG. 2008. Bridging fluorescence microscopy and electron microscopy. Histochem Cell Biol 130(2):211–217.

Goodridge L, Chen JR, Griffiths M. 1999. Development and characterization of a fluorescent-bacteriophage assay for detection of *Escherichia coli* O157: H7. Appl Environ Microbiol 65(4):1397–1404.

Gupta A, Onda M, Pastan I, Adhya S, Chaudhary VK. 2003. High-density functional display of proteins on bacteriophage lambda. J Mol Biol 334(2):241–254.

Hahn MA, Tabb JS, Krauss TD. 2005. Detection of single bacterial pathogens with semiconductor quantum dots. Anal Chem 77(15):4861–4869.

Hahn MA, Keng PC, Krauss TD. 2008. Flow cytometric analysis to detect pathogens in bacterial cell mixtures using semiconductor quantum dots. Anal Chem 80(3):864–872.

Krogmeier JR, Hwang J. 2005. Data analysis considerations in probing single quantum dot fluorescence intermittency. Proc SPIE Int Soc Opt Eng 5705:255–262.

Krogmeier JR, Kang H, Clarke ML, Yim P, Hwang J. 2008. Probing the dynamic fluorescence properties of single water-soluble quantum dots. Opt Commun 281(7):1781–1788.

Mosier-Boss PA, Lieberman SH, Andrews JM, Rohwer FL, Wegley LE, Breitbart M. 2003. Use of fluorescently labeled phage in the detection and identification of bacterial species. Appl Spectrosc 57(9):1138–1144.

Mulholland GW, Donnelly MK, Hagwood CR, Kukuck SR, Hackley VA, Pui DYH. 2006. Measurement of 100 nm and 60 nm particle standards by differential mobility analysis. J Res Natl Inst Stand Tech 111(4):257–312.

Murphy KC. 1998. Use of bacteriophage lambda recombination functions to promote gene replacement in *Escherichia coli*. J Bacteriol 180(8):2063–2071.

Murray NE, Gann A. 2007. What has phage lambda ever done for us? Curr Biol 17(9):R305–R312.

Oda M, Morita M, Unno H, Tanji Y. 2004. Rapid detection of *Escherichia coli* O157: H7 by using green fluorescent protein-labeled PP01 bacteriophage. Appl Environ Microbiol 70(1):527–534.

Pease LF, Tsai DH, Zangmeister RA, Zachariah MR, Tarlov MJ. 2007. Quantifying the surface coverage of conjugate molecules on functionalized nanoparticles. J Phys Chem C 111(46):17155–17157.

Pease LF, Elliott JT, Tsai DH, Zachariah MR, Tarlov MJ. 2008. Determination of protein aggregation with differential mobility analysis: Application to IgG antibody. Biotechnol Bioeng 101(6):1214–1222.

Pomerantsev AP, Sitaraman R, Galloway CR, Kivovich V, Leppla SH. 2006. Genome engineering in *Bacillus anthracis* using Cre recombinase. Infect Immun 74(1):682–693.

Resch-Genger U, Grabolle M, Cavaliere-Jaricot S, Nitschke R, Nann T. 2008. Quantum dots versus organic dyes as fluorescent labels. Nat Methods 5(9):763–775.

Schuch R, Nelson D, Fischetti VA. 2002. A bacteriolytic agent that detects and kills *Bacillus anthracis*. Nature 418(6900):884–889.

Waite-Rees PA, Keating CJ, Moran LS, Slatko BE, Hornstra LJ, Benner JS. 1991. Characterization and expression of the *Escherichia coli* Mrr restriction system. J Bacteriol 173(16):5207–5219.

Wiedensohler A. 1988. An approximation of the bipolar charge-distribution for particles in the sub-micron size range. J Aerosol Sci 19(3):387–389.

Yamaguchi N, Sasada M, Yamanaka M, Nasu M. 2003. Rapid detection of respiring *Escherichia coli*. O157: H7 in apple juice, milk, and ground beef by flo cytometry. Cytom Part A 54(1):27–35.

Yim P, Dobrovolskaia M, Kang H, Clarke M, Patri A, Hwang J. 2007. Nanocrystal-based biomimetic system for quantitative flow cytometry. Proc SPIE Int Soc Opt Eng 6430:64301T.

Zanghi CN, Lankes HA, Bradel-Tretheway B, Wegman J, Dewhurst S. 2005. A simple method for displaying recalcitrant proteins on the surface of bacteriophage lambda. Nucleic Acids Res 33(18):e160.